Some Features of Polymeric Membranes for Water Purification via Membrane Distillation

G. A. Mannella, V. La Carrubba, V. Brucato

Dipartimento di Ingegneria Chimica, Gestionale, Informatica e Meccanica, University of Palermo, Viale delle Scienze, Edificio 6, 90128 Palermo, Italy

Received 28 April 2011; accepted 28 April 2011
DOI 10.1002/app.34765
Published online 10 August 2011 in Wiley Online Library (wileyonlinelibrary.com).

ABSTRACT: Polymeric membranes are currently adopted in water purification processes, such as reverse osmosis (RO) and membrane distillation (MD). This latter technique is very promising for separation effectiveness and energy savings. A valuable and effective MD unit must be equipped with polymeric membranes that exhibit specific properties, for example, hydrophobicity, a narrow pore size range, a high water penetration pressure, and a large vapor permeability. In this work, we present and examine the main features of membranes for MD processes, with the aim of experimentally evaluating the related performances. Scanning electron microscopy analysis was carried out for a first estimate of the pore size distribution; this showed a discrepancy between the nominal pore size and the actual distribution. Vapor flux under typical water purification conditions was measured for different commercial membranes, and values as high as 35 kg m^{-2} h^{-1} were observed. Polytetrafluoroethylene membranes were more permeable for both of the MD configurations tested. The liquid entry pressure (LEP) showed an irreversible decrease in the early operation cycles related to microstructural modifications. A LEP reversible decrease with increasing temperature was observed; this showed that in the membrane selection, the nominal LEP value had to be corrected for the temperature effect for the correct choice. © 2011 Wiley Periodicals, Inc. J Appl Polym Sci 122: 3557–3563, 2011

Key words: membranes; morphology; gas permeation

INTRODUCTION

Polymeric porous membranes are employed in modern technologies for water purification, for example, through reverse osmosis (RO) and membrane distillation (MD).

MD consists of keeping salted hot water in contact with a porous hydrophobic membrane; this confines the liquid and allows the diffusion of water vapor through the pores. The driving force for mass transfer is represented by the difference in vapor pressure between the feed side and the permeate side:[1]

$$N = k_P[P_w^0(T) - P_p] \quad (1)$$

where N is the vapor flux, k_P is the mass-transfer coefficient, $P_w{}^0(T)$ is the water vapor pressure at the operating temperature (i.e., at the feed side), and P_p is the partial pressure of vapor in the permeate side.

Different technologies are available to arrange the vapor recovery from the permeate side:[2] (1) direct contact with a permeate stream (the most widely adopted), (2) sweeping by a noncondensing gas and water recovery in an external condenser, (3) direct vapor condensation by a cool surface, and (4) vapor removal *in vacuo* at a pressure lower than water vapor pressure and subsequent external condensation. The main advantage of MD in water purification is the use of low water temperatures, that is, energy sources, such as waste heat recovery and renewable energy (e.g., thermal and photovoltaic solar energy), that can be integrated in the process layout to generate at least part of the heat needed for the process.[3]

The main features of MD membranes that need to be addressed are the vapor permeability and the liquid entry pressure (LEP); other features, such as effective membrane thermal conductivity, can also be significant. A high vapor permeability is obviously desired to maximize the vapor flux across the membrane, whereas LEP is very important, especially in the vacuum configuration of MD. It is worth noticing that this last configuration leads to the highest vapor flux because the permeate side mass-transfer resistance is the lowest.

Hydrophobic behavior of the membrane for water purification via MD is required to prevent permeate contamination by the membrane pass-through flow

Correspondence to: V. La Carrubba (vincenzo.lacarrubba@unipa.it).

Contract grant sponsors: Regione Siciliana, Assessorato alla Presidenza, Ufficio Speciale per la Cooperazione Decentrata allo Sviluppo ed alla Solidarietà Internazionale, Lympha project.

TABLE I
Membrane Properties and Tests Performed (as Indicated by an X)

Manufacturer	Sample code	Material	Support	NPS (μm)	Thickness (μm)	LEP (bar)	SEM	Vapor flux	LEP
Gore 1	1	PTFE	Spunbonded PP	1	140–340	0.34–0.55 (IPA)	X		
Gore 2	2	PTFE	Spunbonded PP	0.45	180–360	0.62–0.91 (IPA)	X	X	X
Gore 3	3	PTFE	Spunbonded PP	0.20	130–380	0.88–1.59 (IPA)	X	X	
GVS	–	PVDF	Nonwoven polyester	0.20	190–247	2.4–3 (water)	X	X	
Pall 1	1	Acrylic copolymer	Nonwoven nylon	0.20	130–320	1.43 (water)	X		
Pall 2	2	PTFE	Nonwoven polyester	0.20	203–330	1.10–1.79 (IPA)	X		

IPA, isopropyl alcohol.

of the retentate liquid; moreover, the membrane hydrophobicity does not exert a consistent influence on the vapor flux.[4]

A general expression that relates the wetting pressure with the pore size is the Laplace–Young equation:[5]

$$\Delta P_{\text{entry}} = -\frac{2\gamma_i \cos\theta}{r} \quad (2)$$

where ΔP_{entry} is the liquid entry pressure, γ_i is the water surface tension, θ is the contact angle, and r is the pore radius. The surface tension depends on the water temperature and solute concentration, whereas the contact angle is affected by the nature of the membrane material. For a highly hydrophobic material, a θ value of 0° can be assumed. If the membrane has a wide distribution of pore dimensions and shapes, the value of r to consider in the ΔP_{entry} estimation is the highest of the smaller equivalent mean cross-section diameters along any possible pass-through path, instead of the mean value. This aspect has not been thoroughly investigated in MD for desalination, that is, at water temperatures of 50–80°C and at different levels of salinity. LEP is usually measured at ambient temperature (e.g., membrane technical data, see Table I); an example of LEP measurement at different temperatures was carried out with water–alcohol solutions.[5]

Common polymeric materials used are polypropylene (PP), polytetrafluoroethylene (PTFE), or poly(vinylidene fluoride) (PVDF);[6] depending on the polymer, different processes are applied to produce microporous membranes. PVDF membranes are mainly produced via phase inversion,[7] whereas PTFE membranes are fabricated via stretching[8,9] or sintering. PP membranes can be produced by both phase inversion[10] and stretching.

The fabrication technology, in its turn, determines the membrane morphology. For instance, membranes prepared via stretching show a fibrous morphology, where the pores are the open spaces between fibers. On the contrary, membranes produced via phase-separation methods exhibit a network of interconnected pores. The performances of a membrane module for water purification are strictly related to the membrane microstructure. For instance, it has been demonstrated that membrane and support morphologies can affect both the heat and mass transfer.

Membrane characterization is, therefore, a mandatory step before one chooses the appropriate membrane for a MD desalination unit or similar applications. In this article, a survey of the characterization of commercial hydrophobic membranes is presented. The main features, such as morphology, vapor permeability, and LEP, were investigated. The morphology was studied by means of scanning electron microscopy (SEM) micrographs, whereas for vapor flux and LEP, two different dedicated experimental apparatuses were adopted. The comparison of the vapor permeability results with membrane morphologies allowed the recognition of the microstructure to be more suitable for MD desalination. In addition, a case study of LEP measurement is reported; it showed the dependence on the temperature and time of this property.

EXPERIMENTAL

Materials

Six commercial membranes suitable for MD applications were investigated. Table I reports the manufacturers, materials, nominal pore size (NPS), thickness, LEP, and characterizations performed.

SEM

Membrane morphology was visualized by SEM with a Philips 505 microscope. Micrographs were taken of the membrane surface and cross sections. With reference to the sample cross-section preparation before observation, the usually adopted procedure of inducing brittle fracture at liquid nitrogen temperature was not easy to obtain because of the very small membrane thickness. Alternatively, membrane cutting at liquid nitrogen temperature was then applied to preserve its bulk structure.

The pore size distribution of the Pall 1 membrane was determined from the analysis of the SEM micrographs. With regard to the other membranes

studied, the visual discrimination of pores is very difficult: strictly speaking; the fibrous structure did not allow the recognition of distinct pores, which are the free space amid a high number of fibers. In this latter case, gas–liquid porometry offered a way to measure the pore size distribution independently of the membrane microstructure. From the as-obtained distribution, the numerical and weighed average pore sizes were derived,[11] and we calculated the first- and second-order momentum of the distribution, that is

$$D_n = \sum x_i D_i \quad (3)$$

$$D_w = \frac{\sum x_i D_i^2}{D_n} \quad (4)$$

where D_n is the numerical average diameter, x_i is the fraction of pores with diameter D_i, and D_w is the weighted average diameter. The first-order momentum represents the numerical average of the pore diameter; the second-order momentum, divided by the numerical average, is the area-weighted average and is more appropriate to denote the membrane permeability.

Vapor flux

The water vapor permeability of the membranes was measured through a self-built dedicated batch apparatus. It is constituted of a cylindrical vessel (volume $\approx$ 1 L) equipped with an electrical heater (power = 1200 W). A proportional integral derivative (PID) controller (CAL 3200, CAL Controls, Inc., Gurnee, IL) was used to control the liquid temperature. The membrane was placed on one end of the vessel in contact with the liquid hot water, whereas the other face of the membrane was exposed to the atmosphere or closed in a vacuum chamber, depending on the type of measurements to be carried out. The water vapor was removed by forced convection (induced by a fan) or by a Venturi vacuum pump (VP20-100H, VACCON Company, Inc., Medway, MA). The vacuum chamber pressure was measured through a pressure meter (TP704-20BAI, DeltaOHM, S.r.L., 35030 Caselle di Selvazzano (PD) Italy).

In all cases, distilled water was used to prevent the complications induced by the influence of the salt concentration on the process. Moreover, water was boiled for 10 min before testing to eliminate dissolved gases.

We recorded the vapor flux by reading the liquid level in a capillary tube inserted on the lateral surface of the vessel. The slope of the permeate volume versus time curve was used to determine the vapor flow rate throughout the membrane. The experiments were repeated two or more times to test the data reproducibility.

Wetting

LEP was measured through a different self-built dedicated apparatus. It was constituted of a vessel containing hot water continuously recirculated from a thermostatic bath. The membrane was placed on one end of the vessel, in contact with the liquid hot water, whereas the other face of the membrane was exposed to the atmosphere. A brass disk diaphragm was used to reduce the area of the membrane exposed to pressure and to minimize the membrane deformation due to the pressure gap. Moreover, a zinc-coated grid was inserted on the dry face of the membrane to limit the border concentration of stresses, which were potentially responsible for the microstructure modifications. The pressure in the vessel was controlled by a manual valve and measured with a pressure meter (TP704-20BAI, DeltaOHM).

A small amount of methylene blue was added to water as a dyeing agent to allow easy visual detection of liquid membrane pass-through. LEP was detected visually, as small colored water droplets started to appear at a given (reproducible) pressure level. The very low dye concentration did not significantly influence the liquid properties.

LEP was recorded after it reached a constant stationary value. As a matter of fact, when water pressure was applied on the membrane, the LEP value measured was always higher than that after a few cycle of operations. This fact could be explained by the inference that water intrusion into the pores, even in nonwetting cases, modified the membrane microstructure; for example, it caused an enlargement of the pores.[12] For this reason, LEP values were taken only after the stationary and reproducible results were observed.

RESULTS AND DISCUSSION

SEM imaging

The membrane morphologies recorded via SEM imaging were ascribable to two different fabrication technologies:

- Fibrous morphology: Monoaxial stretching [Fig. 1(a)] and biaxial stretching [Fig. 1(b–d)].
- Porous morphology: Phase separation (Fig. 2).

As a matter of fact, the random structure of the PTFE membranes with NPSs of 0.45 and 0.20 μm [Fig. 1(b–d)] should have been related to a biaxial stretching technique,[9] whereas the Gore 1 [Fig. 1(a)] morphology inferred a fabrication via uniaxial stretching[8] because of the ordered and parallel arrangement of the fibers. The Pall 2 membrane exhibited the same structure but a different arrangement of the support. Gore membranes were composed of two clearly distinct layers [Fig. 3(a)], whereas Pall 2 membrane showed the support immersed in two membrane layers [Fig. 3(b)]. The

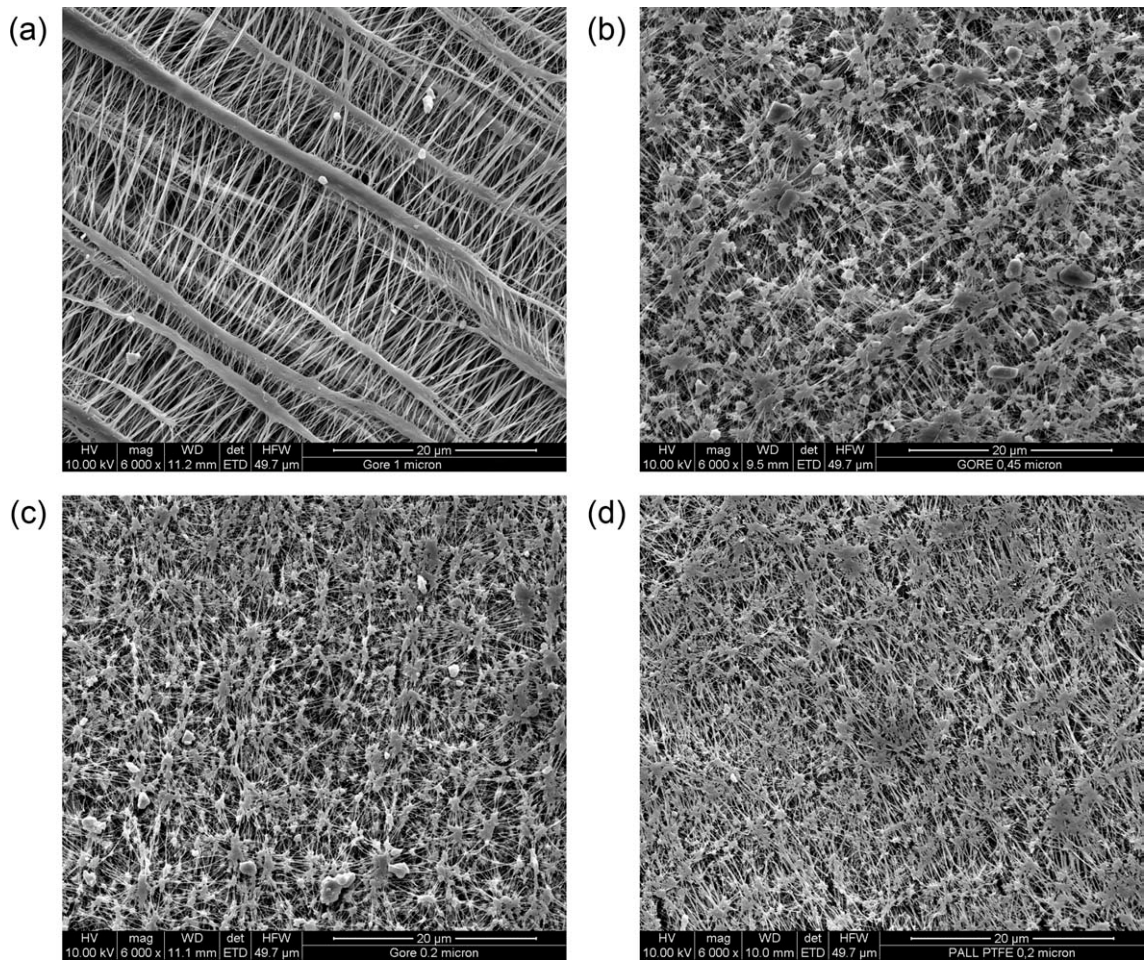

Figure 1 SEM images of membranes fabricated via stretching: (a) Gore, NPS = 1 μm; (b) Gore, NPS = 0.45 μm; (c) Gore, NPS = 0.20 μm; and (d) Pall 2, NPS = 0.20 μm.

Pall and GVS membranes exhibited a similar membrane-support arrangement.

The pore size distribution of the Pall 1 membrane, obtained via image analysis, is shown in Figure 4. As can be readily observed, most of the pores exhibited a diameter larger than NPS (0.20 μm), and the most frequent dimension was about 0.50 μm. On the other hand, the average pore sizes derived via eqs. (3) and (4) were 0.85 and 1.20 μm, respectively. By calculating the area of all pores, we obtained an

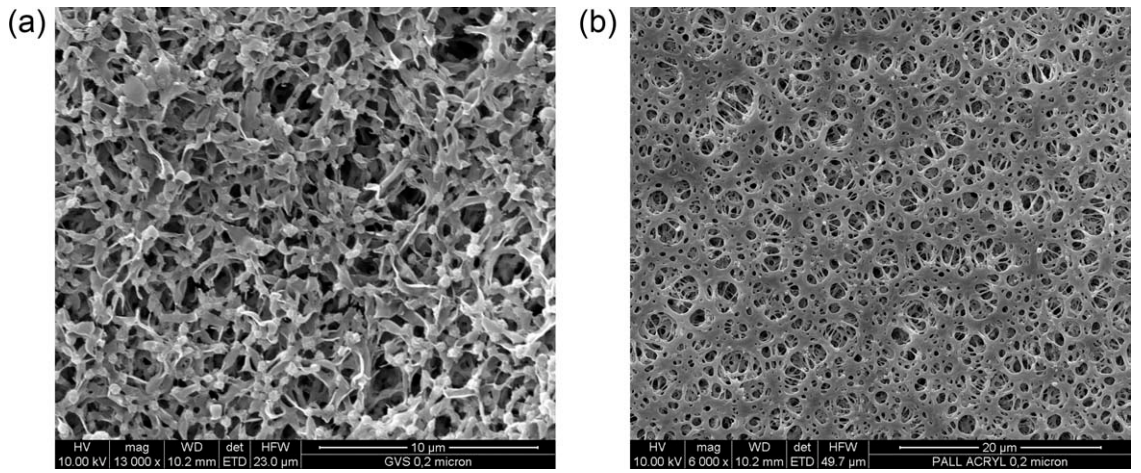

Figure 2 SEM images of membranes fabricated via phase separation: (a) GVS, NPS = 0.20 μm, and (b) Pall 1, NPS = 0.20 μm.

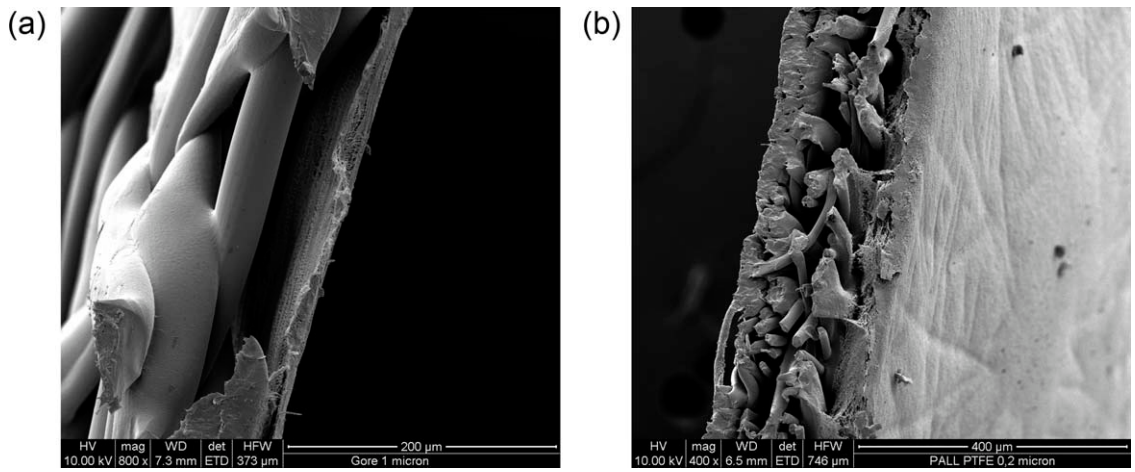

Figure 3 SEM images of transversal sections of the PTFE membranes: (a) Gore, NPS = 1 μm, and (b) Pall 2, NPS = 0.20 μm.

estimate of the surface porosity; for the examined membrane, the porosity value was on the order of 60%.

The presented data refer only to the membrane surface. Although a complete characterization must include the measurement of the pore size and porosity of the whole membrane, for example, via gas–liquid porometry and mercury porosimetry, the information obtained was of some relevance in relation to the MD process. As a matter of fact, the surface properties of the membrane influenced the water flux and membrane fouling.[13] The water flux was directly proportional to the surface porosity: a large area for evaporation increased the vapor flux across the membrane. On the other hand, a small surface porosity (or a small pore size on the surface) reduced the risk of crystal growth into the membrane, that is, fouling.

An experimental study aimed at determining the actual pore size distribution of the membrane was thus mandatory for addressing the design of the membrane modules and to select the appropriate operating conditions. Moreover, the true pore size distribution was a useful additional tool for interpreting and modeling the vapor flux and wetting measurements. It is worth noticing that the LEP referred to the largest pores, which could be wetted under a lower pressure than the smaller pores [see eq. (2)].

Vapor flux

The measured fluxes in the forced convection case (Fig. 5) showed an exponential-like increase with the reciprocal of the temperature; this was in agreement with other works reported in literature.[1,14] This dependence could be explained by consideration of the fact that the driving force for mass transfer [see eq. (1)] exhibited an exponential-like dependence on the temperature. An example of the relation between the vapor pressure (P^0) and temperature is given by the well-known Antoine's equation:

$$P^0 = \exp\left(A - \frac{B}{C+T}\right) \tag{5}$$

where A, B, and C are component-specific constants.

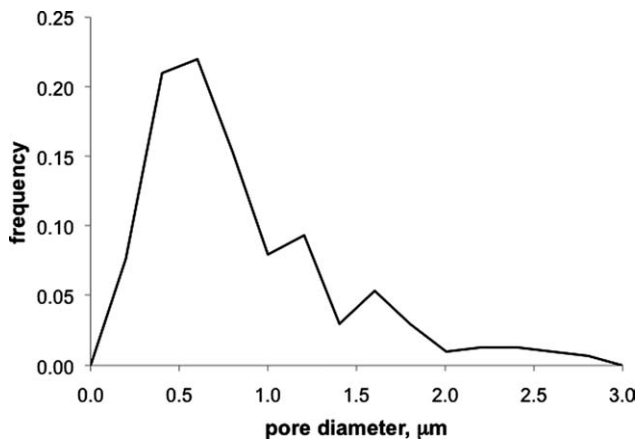

Figure 4 SEM-based pore size distribution of the Pall 1 membrane.

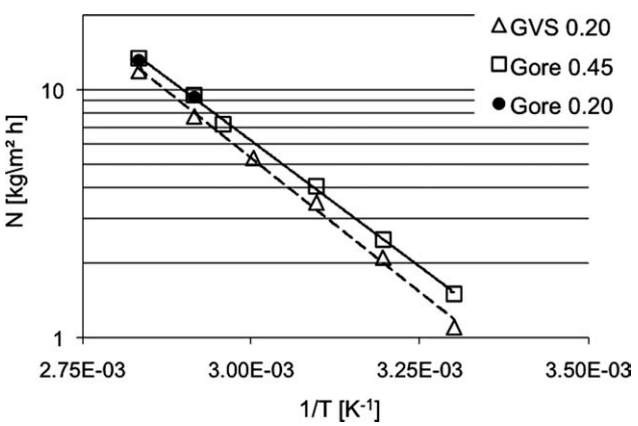

Figure 5 Forced-convection experimental vapor fluxes. Lines are exponential least-squares fitting.

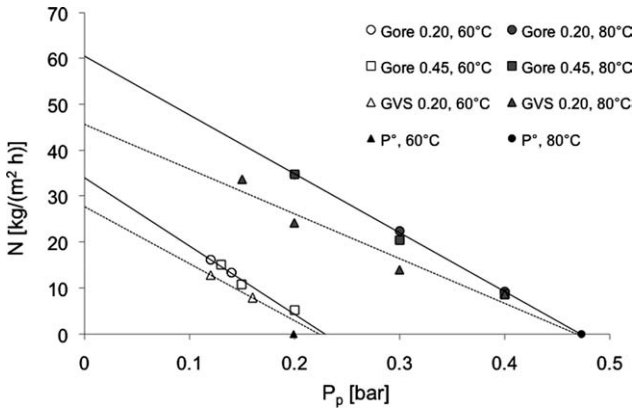

Figure 6 Experimental VMD flux versus permeate chamber pressure. Filled points at $N = 0$ are the water vapor pressures (P^0) at the experimental temperatures.

From these results, a difference between the examined membranes stemmed out immediately. As shown in Figure 5, the fluxes through Gore membranes were slightly higher than in the GVS; this made us speculate about the influence exerted by the membrane material (PTFE vs PVDF) in addition to the role played by pore size. As a matter of fact, in other works,[4,15] PTFE membranes showed better performance than PVDF membranes, although this result was not thoroughly explained by means of material properties (e.g., hydrophobicity effect on liquid meniscus vapor pressure).

The results of the vacuum experiments are presented in Figure 6. In this case, a vapor flux proportional to the pressure difference between the retentate and the permeate side was obtained. All fluxes tended to zero at a permeate pressure close to the water vapor pressure at the given experimental temperatures, as suggested by eq. (1). The highest flux recorded was 35 kg m^{-2} h^{-1}; this was obtained with Gore membranes at $T = 80°C$ and $P_p = 0.2$ bar.

Gore membranes, although different in NPS, showed similar fluxes under the same conditions. However, these membranes could have different porosity values, and an influence of the pore size distribution (rather than the NPS) on the mass transfer was reasonable.

The GVS membrane exhibited fluxes lower than the Gore membranes under the same conditions. This difference between the PTFE and PVDF membranes was reported even for vacuum membrane distillation (VMD) experiments.[15] Moreover, the tortuosity of the PVDF membrane [Fig. 2(a)] appeared to be higher than that of the PTFE membrane [Fig. 1(c)] and presumably affected the vapor mass transfer.

LEP

The results of the LEP measurements for Gore 0.45-μm membrane are displayed in Figure 7. The LEP value decreased with increasing temperature: we explained this result by recalling the depression of the surface tension with increasing temperature [see eq. (2)]. As discussed previously, these values were obtained after a few of operation cycles to reach a steady state by a stabilized pore size.

In general, for a fresh membrane, LEP decreased during the early test cycles, and then, it reached a stationary value. In the first stages of operation, the intrusion of hot water into the pores modified the membrane microstructure. This circumstance must be carefully considered when one performs wetting experiments, as the results can be significantly overestimated, and this will globally lower the process efficiency.

CONCLUSIONS

A survey of the characterization of polymeric membranes for water purification applications was presented. Relevant features, such as the morphology, vapor permeability, and LEP, were investigated.

To choose the appropriate membrane for a given application or to design new membranes for enhancing process performances, many aspects need to be taken into account.

First of all, as the microstructure of the membrane (and also of the support) exerts a sensible influence on the mass and heat transfer, the most suitable morphology for a given application target must be selected, and one must choose among the various membrane production technologies (phase separation and monoaxial and biaxial stretching). As shown by the vapor flux measurements, the PTFE membranes showed better performance than the PVDF membranes; the main reason, although not deeply investigated, should have been related to the membrane morphology. As a matter of fact, both materials were highly hydrophobic, and the material hydrophobicity did not exert a consistent influence

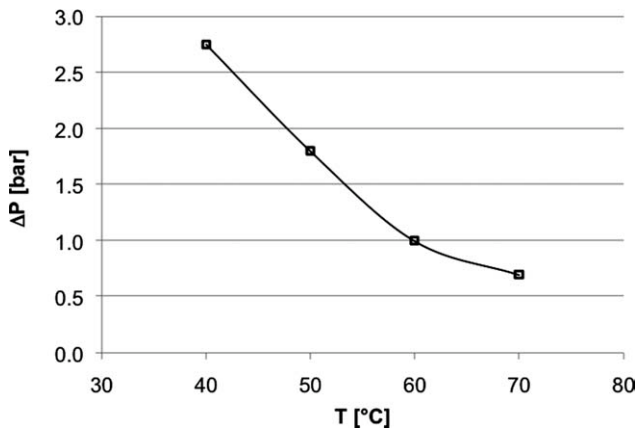

Figure 7 LEP ($\Delta P = P_{feed} - P_{permeate}$) versus temperature for the Gore 0.45 membrane.

on the vapor flux. On the other hand, the membrane preparation techniques, strictly related to the material properties, determined the membrane microstructure. A fibrous morphology had a pore tortuosity lower than that of a network of interconnected pores: this could have been the key value of the PTFE membranes. To double-check this hypothesis, a comparison between membranes made of the same material and fabricated with different techniques could be addressed. To accomplish this study, PP is the most promising polymer, as PP membranes can be fabricated with both phase separation and stretching.

The LEP measurements showed that with increasing temperature, the liquid pass-through became more probable; this circumstance confirmed the usefulness of LEP reliable data at high temperatures (whereas the data sheets included at most the LEP at room temperature), especially for VMD, where the pressure difference across the membrane could be considerably larger than in the other configurations.

The authors kindly acknowledge the precious help of the master students Miriam Bartoli, Alessandro Di Benedetto, Francesco Guttilla, Salvatore Montesanto, and Giuseppe Scaglione for their contribution in carrying out experiments and assembling the vapor flux and LEP measurement system.

References

1. Schofield, R. W.; Fane, A. G.; Fell, C. J. D. J Membr Sci 1987, 33, 299.
2. Li, N. N.; Fane, A. G.; Ho, W. S. W.; Matsuura, T. Advanced Membrane Technology and Applications; Wiley: Hoboken, NJ, 2008.
3. Al-Obaidani, S.; Curcio, E.; Macedonio, F.; Profio, G. D.; Al-Hinai, H.; Drioli, E. J Membr Sci 2008, 323, 85.
4. Zhang, J.; Dow, N.; Duke, M.; Ostarcevic, E.; Li, J.; Gray S. J Membr Sci 2010, 349, 295.
5. Garcia-Payo, M. C.; Izquierdo-Gil, M. A.; Fernandez-Pineda, C. J Colloid Interface Sci 2000, 230, 420.
6. Curcio, E.; Drioli, E. Sep Purif Rev 2005, 34, 35.
7. Hou, D.; Wang, J.; Qu, D.; Luan, Z.; Ren, X. Sep Purif Technol 2009, 69, 78.
8. Kitamura, T.; Okabe, S.; Tanigaki, M.; Kurumada, K.; Ohshima, M.; Kanazawa, S. Polym Eng Sci 2000, 40, 809.
9. Huang, J.; Zhang, J.; Guo, X. H. Y. Eur Polym J 2004, 40, 667.
10. Lin, Y. K.; Chen, G.; Yang, J.; Wang, X. L. Desalination 2009, 236, 8.
11. Kreyszig, E. Advanced Engineering Mathematics; Wiley: New York, 1988.
12. Barbe, A. M.; Hogan, P. A.; Johnson, R. J Membr Sci 2000, 172, 149.
13. Gryta, M. J Membr Sci 2007, 287, 67.
14. Khayet, M.; Godino, P.; Mengual, J. I. J Membr Sci 2000, 170, 243.
15. Mericq, J.-P.; Laborie, S.; Cabassud C. Desalination Water Treatment 2009, 9, 293.